Connecting Thermoelectric Performance and Topological-Insulator Behavior: Bi_2Te_3 and Bi_2Te_2Se from First Principles

Hongliang Shi, David Parker, Mao-Hua Du, and David J. Singh
Materials Science and Technology Division, Oak Ridge National Laboratory, Oak Ridge, Tennessee 37831-6056, USA

(Received 29 July 2014; revised manuscript received 3 December 2014; published 20 January 2015)

Thermoelectric performance is of interest for numerous applications such as waste-heat recovery and solid-state energy conversion and will be seen to be closely connected to topological-insulator behavior. In this context, we here report first-principles transport and defect calculations for Bi_2Te_2Se in relation to Bi_2Te_3. The two compounds are found to contain remarkably different electronic structures in spite of being isostructural and isoelectronic. We discuss these results in terms of the topological-insulator characteristics of these compounds.

DOI: 10.1103/PhysRevApplied.3.014004

I. INTRODUCTION

Thermoelectric performance is typically quantified in term of a dimensionless figure-of-merit ZT given by the following expression:

$$ZT = \frac{S^2\sigma T}{\kappa}. \quad (1)$$

Here, S is the Seebeck coefficient or thermopower, σ is the electrical conductivity, T the absolute temperature, and κ the thermal conductivity. The expression shows that for good performance one desires both a high electrical conductivity and Seebeck coefficient, but these are difficult to obtain simultaneously due to opposite dependencies on carrier concentration. Hence, thermoelectric performance is a counterindicated property of materials that does not commonly occur, and determining and optimizing a usable high-performance thermoelectric material remains a difficult challenge.

Thermoelectric performance is of considerable engineering and technological importance due to the many potential applications of this technology, which include vehicular-exhaust waste-heat recovery, energy harvesting, heating and cooling, and solid-state energy conversion. In all of these applications, higher thermoelectric performance would be extremely beneficial for enhanced device performance. Currently, there are relatively few thermoelectrics with ZT values above unity, the minimum necessary for a thermoelectric to be considered high performance. This has greatly limited the utility of thermoelectrics, leading to substantial efforts aimed at raising ZT.

Presently, the thermoelectric most employed in applications is Bi_2Te_3, a narrow-gap semiconductor which shows optimized ZT figures of approximately unity at ambient temperature. It is presently used primarily in niche applications.

Of great consequence for potential applications at temperatures above 300 K, the performance of Bi_2Te_3 degrades rapidly due to bipolar conduction or the excitation of carriers of both positive and negative charge. This causes the thermopower to decrease with increasing temperature, the opposite of the usual situation, and in addition causes large increases in the electronic thermal conductivity. Both of these effects are destructive for thermoelectric performance, as suggested by Eq. (1). These effects generally occur when the semiconductor band gap (about 0.15 eV in Bi_2Te_3) is not sufficiently large relative to the device operating temperature. In the absence of bipolar conduction, ZT is a strongly increasing function of increasing temperature, with performance ultimately limited only by the decomposition or melting point of the material.

Bi_2Te_3, therefore, could be an extremely high performance thermoelectric at temperatures of 400 to 500 K, if its band gap were only somewhat larger. This would be of great practical importance given that two major potential applications—exhaust waste heat recovery and solid-state thermophotovoltaic conversion—operate at temperatures around 500 K. Part of this work will explore a potential scenario for achieving this.

While Bi_2Te_3 has been known as a high-performance thermoelectric for several decades, it also forms the basis for a family of topological insulators (TI) $(Bi, Sb)_2(Te, Se)_3$ [1]. Many have observed a connection between these two properties and various explanations proposed; perhaps the simplest one is the observation that good thermoelectrics are usually heavy atomic mass small-band-gap semiconductors, as the heavy atom helps to induce low lattice thermal conductivity, as well as the TI band inversion (via spin-orbit coupling), and the small-band-gap high carrier mobility. A floor on the degree of band inversion necessary to produce TI is set by the band gap, presumably making large-band-gap TIs less common.

However, not every, or even a significant fraction of heavy-mass small gap materials, are good thermoelectrics or good TI materials. Furthermore, some materials without heavy-mass atoms or small gaps are excellent thermoelectrics, such as $Mg_2(Si, Sn)$ and Si-Ge. In addition, from an electronic point of view, TI behavior is of interest for an undoped material (where the Fermi energy is in the gap), while high thermoelectric performance is usually observed with the Fermi energy doped into the bulk bands.

Like thermoelectric performance, topologically insulating behavior is of considerable practical importance due to its potential for technological applications, such as memory applications for computers [2]. Here we show a clearer connection between topologically insulating behavior and thermoelectric performance. Briefly, we will see that complex nonparabolic band structures are favorable both for TI behavior and high thermoelectric performance. In this work, we will see that two materials studied as topological insulators—Bi_2Te_3 and Bi_2Te_2Se—appear to have very complex band structures that are, in general, highly beneficial for thermoelectric performance. These complex band structures are related to TI behavior, as the band inversion necessary for this generally creates complex band structures not typically describable in terms of the usual anisotropic effective mass approximation. Remarkably, the two compounds are very different in the near-band-edge electronic structures leading to very different transport behavior.

In Fig. 1, we depict schematically the effects of spin-orbit coupling in producing the complicated band structures just mentioned. Briefly, the band inversion central to TI behavior is induced by spin-orbit coupling, which then opens a gap at the points where the bands would otherwise cross. As depicted in Fig. 1, this generally leads to nonparabolic behavior, often with near-linear Kane band-type dispersions. Thus, a single parabolic nondegenerate band edge, as shown in the left side of Fig. 1, evolves into a nonparabolic complex degenerate band edge, as is often observed in high-performance thermoelectrics. More detailed discussions of these effects can be found in Refs. [3–5].

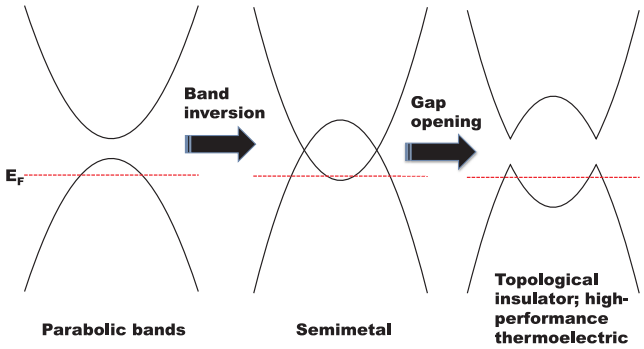

FIG. 1. Depiction of the effects of spin-orbit coupling in generating topologically insulating, potential high-performance thermoelectrics by means of opening of a gap in the electronic structure, with associated nonparabolicity. A material doped *p* type is depicted.

Bi_2Te_3 exhibits the band inversion required for topologically insulating behavior but is inconvenient for studying TI. This is because of its small band gap and small defect-formation energies, which mean that low bulk electrical conductivity—a prerequisite for observing the topologically protected surface states—is difficult to attain. This is due to both large bipolar conduction in the lightly doped intrinsic regime and large band conduction (in the heavily doped extrinsic regime favored by the low vacancy-formation energies). This small band gap also presents a substantial hindrance to thermoelectric applications above room temperature, as bipolar conduction is highly destructive to thermoelectric performance.

Perhaps with this small band gap in mind, significant recent efforts have focused on the topologically insulating properties of the isoelectronic and isostructural Bi_2Te_2Se (experimental band gap of approximately 0.30 eV) where one of the Te layers (see Fig. 2) is entirely replaced with Se. Relatively recently [1], low bulk conductivity single crystals of this material were synthesized and studied, a major step forward towards the experimental verification of the surface states. To date, however, relatively little attention has been directed to the thermoelectric properties of this compound. Indeed, its larger band gap suggests a propensity for thermoelectric performance at temperatures above those of Bi_2Te_3. Disordered alloys near this composition appear to show some potential for thermoelectric performance at higher temperatures but not as high as if the low-T behavior of Bi_2Te_3 could be extended to higher T.

Bi_2Te_2Se forms with a structure closely related to that of Bi_2Te_3. In particular, as shown in Fig. 2, it has a tetradymite-type rhombohedral (space group 166) crystal

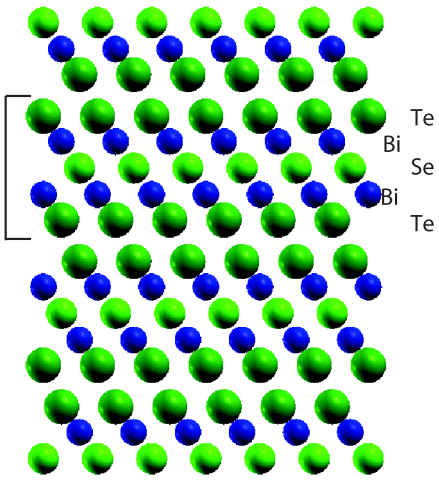

FIG. 2. Depiction of the crystal structure of Bi_2Te_2Se, showing the layer stacking along the rhombohedral *c* axis. The bracket [indicates a single Bi_2Te_2Se layer with Se in the central plane. The atomic positions are taken from the relaxed structure.

structure consisting of Bi_2Te_2Se layers stacked along the c axis and separated by van der Waals gaps. These Bi_2Te_2Se layers are the same as the Bi_2Te_3 layers comprising Bi_2Te_3 except that the central Te plane is replaced by a Se plane [6–8]. Presumably, this particular substitution is favored by the fact that placing Se on this site places this more electronegative atom on the site with the best metal coordination.

The growth of high-quality crystals of this material has recently been perfected, enabling experimental study of its topological-insulating behavior [1,9]. The compound naturally forms as n type from the melt. However, recent experiments show control of the carrier concentration using Sn doping (which introduces midgap states) and excess Bi [1,9,10].

The thermoelectric properties of Bi_2Te_2Se were recently investigated by Fuccillo *et al.* [11]. There has also been recent theoretical and experimental work on the potential performance of nanostructured Bi_2Se_3 and its alloys with Bi_2Te_3 [12,13]. These studies find that Bi_2Se_3 and the compounds between it and Bi_2Te_3 can have higher p-type thermopowers than Bi_2Te_3, especially at temperatures above the operating temperature of Bi_2Te_3, suggesting a propensity for enhanced p-type performance at these temperatures. These studies also suggest that reasonable thermoelectric performance is possible with the reduction of the thermal conductivity by nanostructuring.

II. ELECTRONIC STRUCTURE CALCULATIONS

We perform the present calculations using Boltzmann transport theory with the first-principles electronic structure employing the constant scattering time approximation (see Ref. [14] for a detailed description of this approximation). The BoltzTraP code [15] is used for these transport calculations, and the electronic structure is obtained using the modified Becke-Johnson potential of Tran and Blaha [16]. This potential gives very much improved band gaps for simple semiconductors and insulators as compared to standard density functionals [16–21]. These calculations employ the general potential linearized augmented plane wave method [22], as implemented in the WIEN2k code [23]. Experimental lattice parameters ($a = 4.3792$ Å, $c = 30.00$ Å for Bi_2Te_3, and $a = 4.305$ Å, $c = 30.00$ Å for Bi_2Te_2Se) [8] are used. The free internal atomic coordinates are determined by total energy minimization using the local density approximation (LDA).

The LDA is used because it is found to yield better structural and vibrational properties for Bi_2Te_3 than generalized gradient approximations when used with fixed lattice parameters for Bi_2Te_3 [24]. The structure relaxation is done treating relativity at the scalar relativistic level, as relaxation including spin-orbit coupling is not supported in WIEN; the effect of this omission is likely minimal. All the other reported results include spin-orbit coupling, including the electronic structures and transport properties. Well-converged basis sets defined by a cutoff $RK_{max} = 9.0$ for the plane-wave vector plus local orbitals for the semicore d states are used. Here, k_{max} is the plane-wave cutoff, and R is the sphere radius, which is taken as 2.5 bohr for all atoms.

The calculated band gaps are 0.14 eV for Bi_2Te_3 and 0.22 eV for Bi_2Te_2Se. Thus, the band gap of Bi_2Te_2Se is significantly larger than that of Bi_2Te_3, although still smaller than that of the higher-temperature thermoelectric PbTe (0.36 eV, by a similar method) [25]. The experiment also shows a similar increase in the band gap when Se is added to Bi_2Te_3; i.e., the optical absorption edge is reported to increase from approximately 0.15 eV in Bi_2Te_3 to approximately 0.30 eV at a composition Bi_2Te_2Se [26].

Hinsche *et al.* [27] reported Boltzmann transport calculations for Bi_2Te_3. They found results similar to ours for the thermopower and conductivity, and, in particular, they found better conductivity for the in-plane directions and higher values of the thermopower for p-type doping.

We present the calculated band structure for both materials in Fig. 3. Although some of the features, such as the valence bands more than 0.5 eV below the valence-band maximum, are similar, the fine details of the electronic structure are, in fact, very different. For example, both band extrema for Bi_2Te_3 are at off-symmetry locations [the Bi_2Te_3 valence-band maximum V is approximately (2/5, 2/5, 1/3) in the rhombohedral basis, a nonsymmetry point], while both extrema for Bi_2Te_2Se are at the Γ point. This has important implications for thermoelectric performance, as the increased band degeneracy of Bi_2Te_3 is one likely contributor to its high thermoelectric performance. The valence band of Bi_2Te_3 has two subsidiary maxima

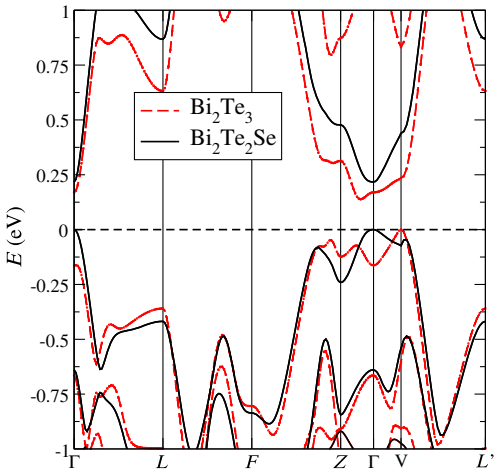

FIG. 3. The calculated band structure of Bi_2Te_3 and Bi_2Te_2Se. We have set the energy 0 to be the valence-band maximum for both materials. The point V refers to the approximate location of the valence-band maximum of Bi_2Te_3—(2/5, 2/5, 1/3) in the rhombohedral basis, and L' to the point (0, 0, −1/2) in the same basis.

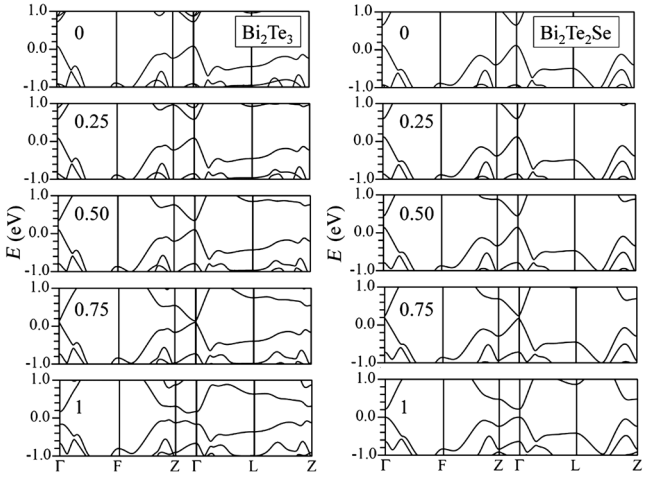

FIG. 4. The calculated band structures of Bi_2Te_3 and Bi_2Te_2Se with the spin-orbit coupling included in strengths (relative to the actual physical value) of 0, 0.25, 0.5, 0.75, and unity.

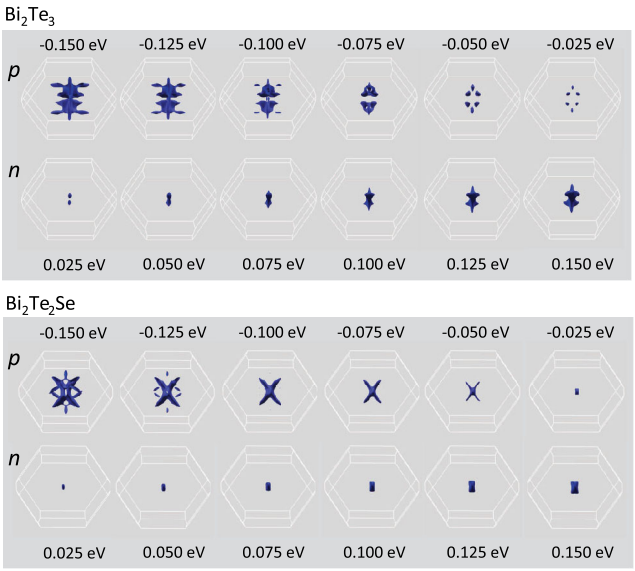

FIG. 5. The calculated isoenergy surfaces of Bi_2Te_3 and Bi_2Te_2Se. The energies given represent the isoenergy value relative to the respective band extrema.

located near the Z point, while Bi_2Te_2Se has two subsidiary valence-band local maxima located at different points.

One plausible question to ask, given the argument of the Introduction for the correspondence between the complex band structures favorable for both thermoelectric performance and topological insulators, is the relationship of the above band structures to spin-orbit coupling. In order to address this question, we present in Fig. 4 the results of the calculations in which the effective strength of the spin-orbit coupling is varied from zero to unity (the fully-spin-orbit case). As the plots indicate, without spin-orbit, both materials are direct-gap semiconductors with band edges at the Γ point and comparatively parabolic bands. In both cases, however, as the spin-orbit interaction is turned on, the band gap decreases radically until in the 0.75 plot the gap is very small—less than a tenth of an electron volt, and the bands become visibly nonparabolic. Finally, as in the right-hand panel of Fig. 1, when the full strength of the spin-orbit is applied, a new gap opens up between the Z and Γ points for Bi_2Te_3 but returning to the Γ point for Bi_2Te_2Se, and these band structures do appear to be comparatively nonparabolic. Note also that the motion of the band edges in Bi_2Te_3 away from the Γ point with the advent of spin-orbit automatically implies a more complex Fermi surface structure due to the associated degeneracy, irrespective of the parabolicity of the bands.

By way of comparison, the band structure of Bi_2Te_2Se is, in fact, much more similar to that of Bi_2Se_3, which also has both extrema at the Γ point, than that of Bi_2Te_3, despite being closer to the latter compound compositionally. Further insight can be obtained by plotting the isoenergy surfaces of both materials, as presented in Fig. 5. For both materials, for p-type doping, a highly anisotropic nonparabolic behavior is evident. Recall that in a parabolic approximation, the isoenergy surfaces take the form of ellipsoids of revolution, even if effective mass anisotropy is considered. Neither of these materials exhibits a p-type Fermi surface at all resembling an ellipsoid; for Bi_2Te_3, at the smallest energies, a distinct triangular shape appears followed at increasing binding energy by a bell-like structure and ultimately augmented with planar "wings." The shape is very different for Bi_2Te_2Se, with the initial VBM at Γ rapidly evolving into an X-shaped figure (note that there are, in fact, six subsidiary extrema in this structure), which is then followed by a ringlike feature.

All of these deviations from spherical or ellipsoidal shapes can be seen to be beneficial for thermoelectric performance. For a given volume (in this case, effectively carrier concentration), a sphere has the minimum surface area [in this case, effectively density of states (DOS)] and, therefore, minimum thermopower, since in the degenerate limit the thermopower is proportional to the DOS mass. Hence, all deviations from a spherical isoenergy surface enhance the thermopower, and the greater the deviation, the greater the enhancement. An example of this effect can be found in Ref. [28]. While a detailed quantitative comparison between the two materials on this basis is not readily available, we may state with some confidence that both materials, when doped p type, will benefit from the anisotropy of the electronic structure.

With regards to n type, here the situation is substantially different. While Bi_2Te_3 still affords a substantially anisotropic isoenergy surface with a discus shape evolving out of a non-Γ-point extremum, for Bi_2Te_2Se there is only a single Γ-centered relatively cylindrical extremum, and this cylindrical shape is notably "closer" to a spherical shape than that of Bi_2Te_3. Hence, we expect, and will later see,

diminished n-type performance for Bi_2Te_2Se relative to Bi_2Te_3.

We note that all band structures are significantly different from the "pudding-mold" band structure proposed by Kuroki and Arita [29] as an explanation for the simultaneous occurrence of high thermopower and electrical conductivity in the cobalt state Na_xCoO_2. In that band structure, a flat upper portion provides the large density of states necessary for a high Seebeck coefficient, while a dispersive portion connecting to this provides a light band which favors high conductivity. Here, Bi_2Te_3, in particular, from Figs. 3 and 5, contains near-degenerate band edges resulting from its complex isoenergy surfaces that allow it to attain high conductivity without sacrificing thermopower, a distinct scenario from that of Ref. [29].

Although it is not immediately apparent from the plots, the isoenergy surfaces reflect the rhombohedral symmetry, with the off-symmetry valence-band maximum for Bi_2Te_3 sixfold degenerate and the conduction band minimum located on the trigonal axis twofold degenerate. For p-type Bi_2Te_2Se, the X emanating from the Γ point (beginning at −0.005 eV) actually comprises six "arms," as two of the arms are hidden by the projection.

III. BOLTZMANN TRANSPORT CALCULATIONS

Following the electronic structure calculations, we perform Boltzmann transport calculations of the doping and temperature-dependent thermopower and electrical conductivity, within the "constant-scattering time approximation," which shows substantial success in describing the thermopower of a large number of materials. Within this theory of diffusive transport, the expressions for the thermopower and conductivity are

$$S = \frac{\int dE\sigma(E)(E - E_F)f'(E - E_F)}{\int dE\sigma(E)f'(E - E_F)} \tag{2}$$

and

$$\sigma = \int dE\sigma(E)f'(E - E_F), \tag{3}$$

where f' is the energy derivative of the Fermi function, $\sigma(E)$ is the energy-dependent transport function related to conductivity, $N(E)\langle v^2(E)\tau(E)\rangle$, $N(E)$ the density of states, v^2 the square of the component of the band velocity on the direction of the interest (i.e., v_x for conductivity along direction x, making v^2 a rank-2 tensor, like the conductivity), and τ the inverse scattering rate. The constant-scattering time approximation is the neglect of the energy (but not doping or temperature) dependence of τ, so that the transport function becomes $N(E)\langle v^2(E)\rangle\tau$, where $\langle v^2\rangle$ is the average Fermi velocity (still a rank-2 tensor).

With these preliminaries complete, we move to the calculated quantities of interest. In Fig. 6, we present the thermopower for the two materials at three temperatures:

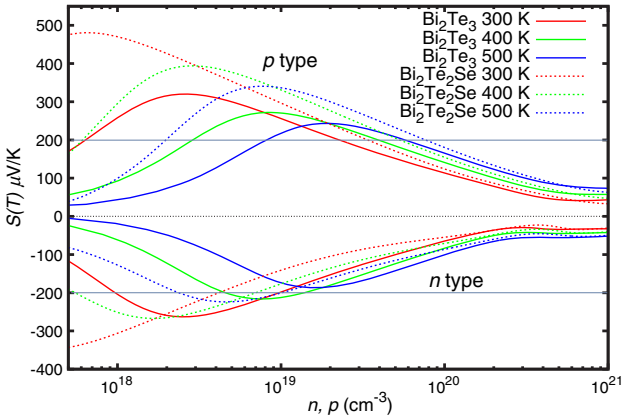

FIG. 6. Conductivity-averaged Seebeck coefficient as a function of carrier concentration for Bi_2Te_3 (solid lines) and Bi_2Te_2Se (dashed lines) for p-type (above zero line) and n-type doping (below zero line) levels. The horizontal blue lines indicate a thermopower magnitude of 200 μV/K, generally the minimum necessary for a material to be a high-performance thermoelectric.

300, 400, and 500 K. Note that due to the anisotropy of the electronic structure, we depict the conductivity-weighted thermopower as would be observed in the polycrystalline sample typically measured in the experiment. For p type, one notes that the thermopower is significantly larger for Bi_2Te_2Se than for Bi_2Te_3, as a function of carrier concentration, for all three temperatures. This reflects the differing electronic structure of these two materials, as well as the larger calculated band gap of Bi_2Te_2Se. At all three temperatures, p-type Bi_2Te_2Se displays a substantial range of carrier concentration where the thermopower is larger than 200 μV/K. As we note elsewhere [30], the Wiedemann-Franz relation essentially necessitates a thermopower magnitude of 200 μV/K or greater for a high-performance thermoelectric; it is worth noting that this is the 300-K thermopower of optimally doped Bi_2Te_3. For n type, the thermopower of Bi_2Te_2Se appears inferior to that of Bi_2Te_3, even with the larger band gap, presumably due to the less anisotropic and, hence, less nonparabolic electronic structure. We, therefore, focus on p-type behavior in the following.

The benefits of Bi_2Te_2Se relative to Bi_2Te_3 in the p-type thermopower should not, however, necessarily be taken as quantitative evidence for likely better, or even equal, thermoelectric performance in Bi_2Te_2Se. In order to assess this, we plot the average electrical conductivity versus thermopower at 300 K in Fig. 7. Figure 7 reveals that in the p-type (right-hand side of plot) region of thermopower around 200 μV/K, the two materials have virtually identical σ/τ, which will indicate comparable thermoelectric transport if the scattering times are equal. The same behavior is evident at 500 K (not shown). Note that in this comparison, we are not referring to the bottom portion of the graphs, near where the thermopower transitions from positive to negative. This region is firmly within the bipolar

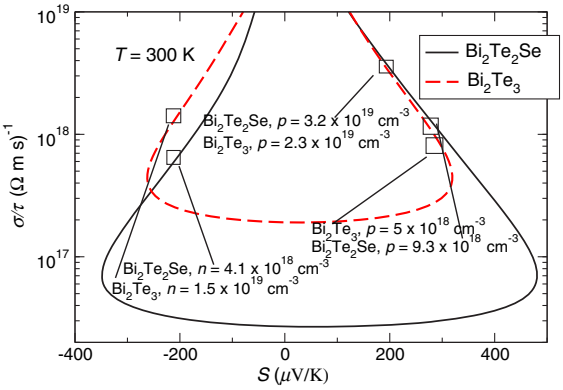

FIG. 7. Average 300-K conductivity versus the Seebeck coefficient for Bi_2Te_3 (dashed lines) and Bi_2Te_2Se.

regime, well below optimal doping, and for which thermoelectric performance is generally poor. Instead, we refer to the linear region adjacent to the legend, which is likely near where optimal performance would be found.

The isoenergy surfaces for p-type Bi_2Te_2Se appear to be somewhat less anisotropic than for Bi_2Te_3, which may explain why the thermopower benefits versus carrier concentration do not remain when compared to σ/τ. With regards to τ, the scattering times may not be equal, given that in one sample of the line compound Bi_2Te_2Se disorder [1] of order 5% is observed on the Te/Se sites, which tends to decrease scattering times and, hence, electrical conductivity. Optimal electrical conductivity in Bi_2Te_2Se, therefore, may necessitate extremely careful sample preparation in order to minimize this effect.

For a further comparison, in Fig. 8 we depict the calculated power factor $S^2\sigma/\tau$ (with respect to an average unknown scattering time) at 300 K for both materials, for p type and n type, as a function of carrier concentration (carriers per unit cell). The plot depicts comparable behavior for p type, consistent with the behavior in Figs. 6 and 7, noting that shorter scattering times in Bi_2Te_2Se may degrade the performance of this material relative to that of Bi_2Te_3. For n type, this figure suggests,

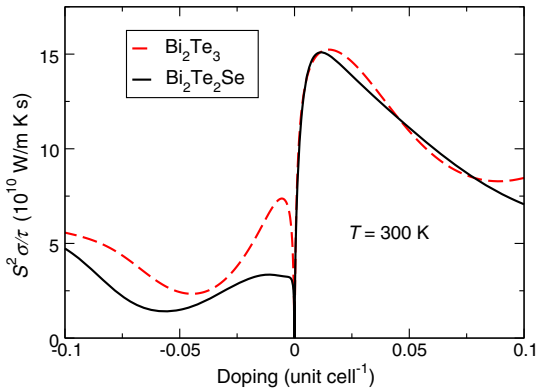

FIG. 8. Average 300-K power factor $S^2\sigma/\tau$ versus the doping level for Bi_2Te_3 (solid lines) and Bi_2Te_2Se.

consistent with the other figures, that Bi_2Te_2Se performance will significantly lag behind that of Bi_2Te_3.

Returning to Fig. 6, p-type Bi_2Te_3 shows doping levels where the thermopower is above 200 μV/K at temperatures above 300 K, where thermoelectric performance is usually believed to deteriorate. This is most significant at 400 K but is true even at 500 K. This means good thermoelectric performance may be obtained at these temperatures. Actual results, particularly at 500 K, will depend sensitively on the exact value of the band gap at these temperatures, as well as on any differences in hole and electron scattering times. Performance will likely be optimized at dopings significantly heavier than those (about $p = 2 \times 10^{19}$ cm^{-3}) used for commercial Bi_2Te_3. This is necessary to minimize bipolar conduction. At 400 K, this doping level is approximately 4×10^{19} cm^{-3} and at 500 K, it is 5.8×10^{19} cm^{-3}. Because of the close proximity of the bipolar regime, performance will rapidly degrade at dopings below these. For n type, there is no such region of extended higher-temperature performance for either Bi_2Te_3 or Bi_2Te_2Se.

Figures 6–8 together suggest that the likelihood of Bi_2Te_2Se performance exceeding that of Bi_2Te_3 is fairly low, even at the elevated temperatures where its larger band gap is expected to be an advantage. This has implications for the ongoing search for technologically useful thermoelectrics in the 400 to 500 K range, in particular, suggesting that a larger band gap cannot necessarily be considered a panacea for achieving high thermoelectric performance. In this case, it is the less-favorable electronic structure of Bi_2Te_2Se relative to Bi_2Te_3 that is the source of the difficulty, suggesting that even closely related materials are not necessarily equivalent from the standpoint of thermoelectric performance.

We note that, presumably due to the weakly bonded van der Waals layers in both these materials, the lattice parameters determined from a first-principles optimization can differ significantly from the experimental lattice parameters used in the foregoing calculations (see Table I for the actual values). Given this, it is natural to perform an assessment of the effects of such differences on electronic structure and on the transport quantities depicted in the above plots. We depict such a comparison in Fig. 9 above, for the planar thermopower at 300 K. For p type, the results depict a marginal decrease in Bi_2Te_3 thermopower and equally marginal increase in Bi_2Te_2 thermopower; the main effect of the smaller theoretical lattice parameters is, in fact, an increase in the calculated band gap of Bi_2Te_2Se by approximately 0.06 eV. This change, however, affects only the thermopower for Bi_2Te_2Se at dopings around 10^{18} cm^{-3}, far below optimal doping, so for the purposes of assessing thermoelectric performance, the effects on the p type of the theoretical lattice parameters are essentially nil. With regards to n type, the effects of the experimental lattice parameters are somewhat larger but are of similar magnitude

TABLE I. The lattice constants we use in this work.

	Bi[a]	Se[b]	Te[c]	Bi_2Se_3[d]	Bi_2Te_3	Bi_2Te_2Se
Experimental a	4.546	4.368	4.458	4.135	4.379	4.305
Experimental c	11.862	4.958	5.925	28.615	30.481	30.00
Theoretical a	···	···	···	···	4.350	4.265
Theoretical c	···	···	···	···	29.82	29.33

[a]Experimental value in Ref. [31].
[b]Experimental value in Ref. [32].
[c]Experimental value in Ref. [33].
[d]Experimental value in Ref. [34].

(and the same sign) for both materials, so that on a comparative basis, here too the effects are rather small. Finally, we note that the use of the experimental lattice parameters generally gives better agreement with experiment in these van der Waals materials and so retain their usage for the electronic structure calculations presented here.

IV. LATTICE DYNAMICS CALCULATIONS

Lattice dynamics, or phonon band structure and transport, ultimately determines the lattice thermal conductivity, a key quantity affecting thermoelectric performance. To this end, we perform lattice dynamics calculations for Bi_2Te_2Se using density functional theory in Blöchl's projector augmented-wave (PAW) method within the LDA as implemented in VASP. A $3 \times 3 \times 3$ k-point grid in a $3 \times 3 \times 3$ supercell is used, along with an energy cutoff of 300 eV. The cell parameters and internal coordinates are both relaxed until the internal forces are less than 2 meV/ Å. The optimized lattice constants for Bi_2Te_2Se are $a =$ 4.265 Å and $c = 29.328$ Å.

In Figs. 10 and 11, we present the phonon band structure and site-projected density of states for Bi_2Te_2Se. Note that in Figs. 10 and 11 we also include a band structure and density of states for Bi_2Te_3 calculated from one of our previous works using the same methods. We immediately note a great similarity in the phonon band structures, with the main difference being slightly larger frequencies in Bi_2Te_2Se and a somewhat larger gap in the (2–2.5)-THz

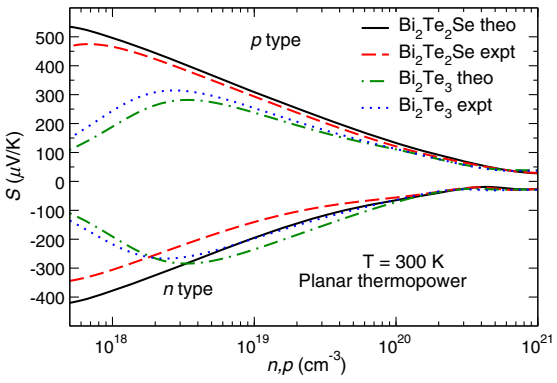

FIG. 9. Planar thermopower values for Bi_2Te_3 and Bi_2Te_2Se, using both the experimental and theoretical lattice parameters.

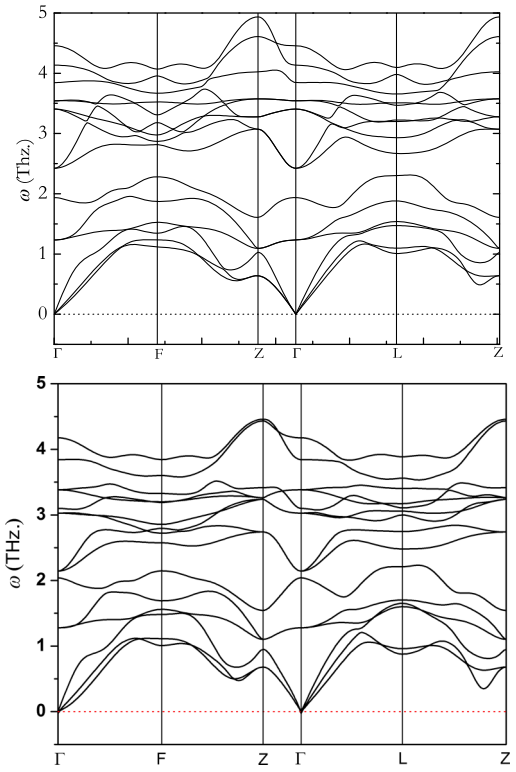

FIG. 10. Computed phonon band structure for Bi_2Te_2Se (top) and Bi_2Te_3 (bottom) from Ref. [24]. The coordinates of the high symmetry points are (in units of the rhombohedral lattice vector) L (1/2, 0, 0), F (1/2, 0, 1/2), and Z (1/2, 1/2, 1/2).

region in Bi_2Te_2Se. It is noteworthy that the phonon band structures are so similar, while the electronic band structures are so different. Part of this is that phononic transport tends to be less variable than electronic, but a more fundamental reason is that for thermoelectrics and topologically insulators, only the region near the band extrema is of relevance, and these can clearly vary more widely than the entire electronic structure. The sound speeds for Bi_2Te_2Se are somewhat higher than for Bi_2Te_{f3}; in the nearly planar Γ-L direction, the Bi_2Te_2Se sound speeds (transverse modes first) are 1524, 1763, and 2500 m/ sec, while the corresponding values for Bi_2Te_3 are 1395, 1728, and 2394 m/ sec. For the c-axis Γ-Z direction, the values for Bi_2Te_2Se are 1781 (degenerate transverse mode) and 1994 m/ sec, and the corresponding values for Bi_2Te_3 are 1774 and 1811 m/ sec. The significantly lighter mass of Se relative to Te is likely responsible for the higher phonon frequencies and sound speeds of Bi_2Te_2Se.

Given the higher sound speeds, the lattice thermal conductivity of Bi_2Te_2Se may be somewhat higher than that of Bi_2Te_3. Note, however, that the sound speeds for Bi_2Te_2Se are still comparatively low, so that fairly low lattice thermal conductivity can be expected in the Bi_2Te_2Se material. The lower-longitudinal c-axis sound speed suggests somewhat lower thermal conductivity in this direction than in plane.

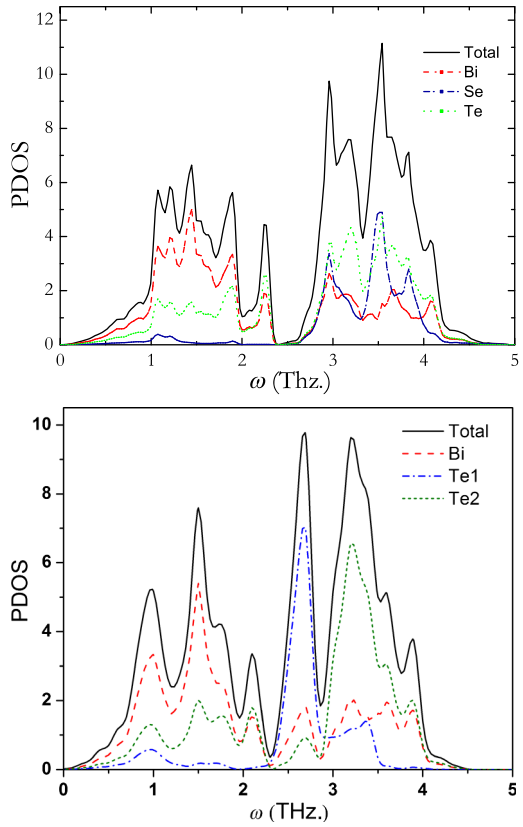

FIG. 11. Computed phonon density of states for Bi_2Te_2Se (top) and Bi_2Te_3.

Moving to the calculated phonon density of states (Fig. 11), we note immediately the prominent Se peak around 3.5 THz, near the top end of the spectrum. This is reasonable considering the lower mass of Se relative to Te and Bi. The lower-frequency modes below 2.5 THz are most predominantly Bi, which again comports with the extremely heavy mass of Bi. One final point of interest is that there is a nearly complete gap opened around 2.5 THz. This gap is more prominent than in Bi_2Te_3, and this is again likely a result of the lighter Se atom increasing the frequency of the highest modes found between 2.5 and 4 THz. This also can be seen in Fig. 10, where for Bi_2Te_2Se there is a gap of approximately 0.3 THz at the Γ point but essentially no gap at this point in Bi_2Te_3.

It is of interest to compare the behavior of the Se atom partial DOS in Bi_2Te_2Se in Fig. 11 (top) with that of Te1 in Bi_2Te_3 in Fig. 11 (bottom), since these two atoms occupy the same between-layer site (see Fig. 2). As the figure indicates, the Te1 DOS is almost entirely (excepting the acoustic regime) comprised of a single peak around 2.7 GHz, while the Se DOS is comprised of three separate peaks at 3, 3.5, and 3.8 GHz. All these Se peaks' energies are higher than the Te1 peak in Bi_2Te_3, as expected given the lighter mass of Se, but the split in these Se peaks is of interest. We suspect its origin is the effectively more complex physical structure of Bi_2Te_2Se in containing three distinct atomic masses rather than two, which splits what would otherwise be a more singular peak.

V. DEFECT-ENERGY CALCULATIONS AND PHASE STABILITY

It is well known that Bi_2Te_3 tends to form off stoichiometry due to low antisite defect-formation energies [35]. Within this context, it is of interest to consider the defect-formation energies in Bi_2Te_2Se as these will provide important information about the nature and magnitudes of defect formation and associated scattering in this material. We limit ourselves to Se and Te antisite defects, as due to the equivalent charge count, these energies are expected to be especially low.

These defect calculations, as with the lattice dynamics calculations, are based upon density functional theory in the framework of Blöchl's PAW method within the LDA as implemented in VASP. We use a $4 \times 4 \times 1$ conventional hexagonal unit cell containing 240 atoms and the $2 \times 2 \times 1$ Monkhorst-Pack k-point grid together with an energy cutoff of 500 eV. The force convergence criterion acting on atoms is less than 0.01 eV/Å. The experimental lattice constants are used for Bi_2Te_2Se, Bi_2Te_3, Bi_2Se_3, Bi, Se, and Te as listed in Table I.

For the defect calculations, the formation energies ΔH for the defect in the charge state q are given by

$$\Delta H_{D,q}(E_F,\mu) = (E_{D,q} - E_H) + \sum_\alpha n_\alpha(\Delta\mu_\alpha + \mu_\alpha^{\text{solid}}) + q(E_v + E_F). \quad (4)$$

Since we concern ourselves only with the Se_{Te} and Te_{Se} antisite defects with the same valence states, q equals 0.

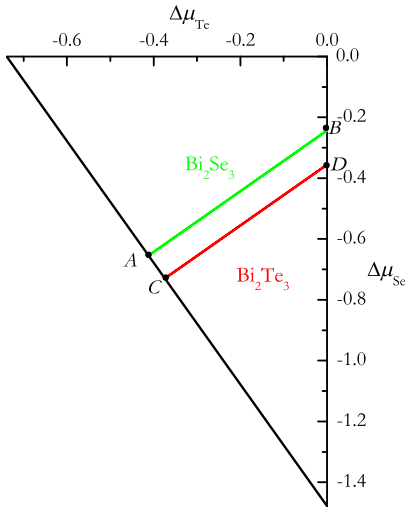

FIG. 12. Calculated ranges of chemical potentials of the elements involved in Bi_2Te_2Se and related competing phases. The range of thermodynamical stability of Bi_2Te_2Se is defined by the trapezoid *ABCD*.

TABLE II. The calculated defect-formation energies for antisite defects Se_{Te} and Te_{Se} with chemical potentials at A, B, C, D points.

	A	B	C	D
$(\Delta\mu_{Te}, \Delta\mu_{Se})$	$(-0.41, -0.65)$	$(0, -0.24)$	$(-0.37, -0.73)$	$(0, -0.36)$
Se_{Te}	0.115	0.115	0.228	0.228
Te_{Se}	0.154	0.154	0.041	0.041

In the first term, $E_{D,q}$ and E_H are the total energies of a solid with and without defect D, respectively. The second term represents the energy of the atom of species α added ($n_\alpha = -1$) or removed ($n_\alpha = 1$) from a reservoir of that species with chemical potential $\mu_\alpha = \Delta\mu_\alpha + \mu_\alpha^{\text{solid}}$.

Under equilibrium conditions for the crystal growth, the chemical potentials μ_α must satisfy certain conditions in order to form a stable host compound. Other competing phases (including elemental solids) must be avoided. In order to maintain the stability of Bi_2Te_2Se during growth and avoid competing phases (e.g., Bi, Te, Se, Bi_2Te_3, and Bi_2Se_3), the relative chemical potential $\Delta\mu_\alpha$ must satisfy the following limits:

$$2\Delta\mu_{Bi} + 2\Delta\mu_{Te} + \Delta\mu_{Se} = \Delta H(Bi_2Te_2Se) = -1.478 \text{ eV}, \tag{5}$$

$$\Delta\mu_{Bi} \le 0, \qquad \Delta\mu_{Te} \le 0, \qquad \Delta\mu_{Se} \le 0, \tag{6}$$

$$2\Delta\mu_{Bi} + 3\Delta\mu_{Te} \le \Delta H(Bi_2Te_3) = -1.123 \text{ eV}, \tag{7}$$

$$2\Delta\mu_{Bi} + 3\Delta\mu_{Se} \le \Delta H(Bi_2Se_3) = -1.964 \text{ eV}. \tag{8}$$

All calculated heats of formation of ternary and binary compounds in this work are given per formula unit.

Equations (5)–(8) are projected to the two-dimensional panel with two independent variables $\Delta\mu_{Te}$ and $\Delta\mu_{Se}$, as shown in Fig. 12. The thermodynamically stable ranges of chemical potentials of the elements in Bi_2Te_2Se (trapezium, $ABCD$) are obtained by excluding the regions of chemical potentials in which competing phases are thermodynamically stable, as shown in Fig. 12.

Our calculated formation energies of antisite Se_{Te} and Te_{Se} are are collected in Table II, with relative chemical potentials at the corresponding A, B, C, and D points in Fig. 12.

Figure 12 asserts that Bi_2Te_2Se is only thermodynamically stable within a narrow Te-Se compositional range, above which Bi_2Se_3 will be formed and below which Bi_2Te_3 will be formed. From Table II, we see that certain defect structures such as Te_{Se} have defect energies as low as 0.041 eV. When one considers putative synthesis conditions of 1000 K, this will in equilibrium yield a Te_{Se} defect concentration of order 50%, an absurdly large number. Hence, it will be important to synthesize under conditions towards the Se-rich side. Even here, though, the defect-formation energies are low, 0.115 eV for Se_{Te} defects and 0.154 eV for Te_{Se} defects, both less than twice the thermal energy at 1000 K, so that substantial numbers of defects are likely to be formed at typical synthesis conditions.

There are two main points to be gleaned from these results. First, since the defect-formation energies are small and asymmetric, substantial numbers of defects will form, and the number of Te_{Se} and Se_{Te} defects will not be equal, so the material will likely form off stoichiometry. Second, and more important, since the electronic structures of the two compounds Bi_2Te_3 and Bi_2Te_2Se are so different, these large numbers of defects are likely to induce substantial alloy scattering, which is likely to significantly impair mobility. It may also reduce the lattice thermal conductivity, but given that this is already likely to be fairly low, the mobility reduction is likely to be the larger effect.

VI. CONCLUSION

Topological insulators, such as Bi_2Te_3 and Bi_2Te_2Se considered in this work, of necessity have complex band structures due to the band inversion central to the topologically insulating behavior. These complex band structures, in particular, highly nonparabolic isoenergy surfaces, are also those favored by high-performance thermoelectrics, and these two studied materials appear to contain such anisotropic features, though rather different in the specifics. The relationship between thermoelectric performance and TI behavior is, thus, through the band structure as it relates to transport. TI materials necessarily have highly nonparabolic shapes that generally lead to corrugated isoenergy surfaces at the doping levels of interest for thermoelectrics. These corrugated surfaces are favorable for obtaining the combination of high conductivity and high thermopower required in a high-performance thermoelectric.

The favorability of complex nonparabolic band structures for both TI behavior and high thermoelectric performance suggests that future searches for such technologically promising materials may benefit from a consideration of the degree of complexity and anisotropy of the electronic structure of materials studied. It will be of interest to pursue these potentially useful behaviors from this perspective.

ACKNOWLEDGMENTS

This work is sponsored by the U.S. Department of Energy, Basic Energy Sciences, Materials Science and Engineering Division (H. S. and M. H. D.) and the DOE S3TEC Energy Frontier Research Center (D. P. and D. J. S.).

[1] S. Jia, H. Ji, E. Climent-Pascual, M. K. Fuccillo, M. E. Charles, J. Xiong, N. P. Ong, and R. J. Cava, Low carrier-concentration crystals of the topological insulator Bi_2Te_2Se, Phys. Rev. B **84**, 235206 (2011).

[2] A. R. Mellnik, J. S. Lee, A. Richardella, J. L. Grab, P. J. Mintun, M. H. Fischer, A. Vaezi, A. Manchon, E. A. Kim, N. Samarth, and D. C. Ralph, Spin-transfer torque generated by a topological insulator, Nature (London) **511**, 449 (2014).

[3] D. Hsieh, Y. Xia, D. Qian, L. Wray, F. Meier, J. H. Dil, J. Osterwalder, L. Patthey, A. V. Fedorov, H. Lin, A. Bansil, D. Grauer, Y. S. Hor, R. J. Cava, and M. Z. Hasan, Observation of time-reversal-protected single-Dirac-cone topological-insulator states in Bi_2Te_3 and Sb_2Te_3, Phys. Rev. Lett. **103**, 146401 (2009).

[4] Y. L. Chen, J. G. Analytis, J.-H. Chu, Z. K. Liu, S.-K. Mo, X. L. Qi, H. J. Zhang, D. H. Lu, X. Dai, Z. Fang, S. C. Zhang, I. R. Fisher, Z. Hussain, and Z.-X. Shen, Experimental realization of a three-dimensional topological insulator, Bi_2Te_3, Science **325**, 178 (2009).

[5] H. Zhang, C.-X. Liu, X.-L. Qi, X. Dai, Z. Fang, and S.-C. Zhang, Topological insulators in Bi_2Se_3, Bi_2Te_3 and Sb_2Te_3 with a single dirac cone on the surface, Nat. Phys. **5**, 438 (2009).

[6] J. R. Wiese and L. Muldawer, Lattice constants of Bi_2Te_3-Bi_2Se_3 solid solution alloys, J. Phys. Chem. Solids **15**, 13 (1960).

[7] S. Nakajima, The crystal structure of $Bi_2Te_{3-x}Se_x$, J. Phys. Chem. Solids **24**, 479 (1963).

[8] S. Misra and M. B. Bever, On the solid solutions of bismuth telluride and bismuth selenide, J. Phys. Chem. Solids **25**, 1233 (1964).

[9] Z. Ren, A. A. Taskin, S. Sasaki, K. Segawa, and Y. Ando, Fermi level tuning and a large activation gap achieved in the topological insulator Bi_2Te_2Se by Sn doping, Phys. Rev. B **85**, 155301 (2012).

[10] S. Jia, H. Beidenkopf, I. Drozdov, M. K. Fuccillo, J. Seo, J. Xiong, N. P. Ong, A. Yazdani, and R. J. Cava, Defects and high bulk resistivities in the bi-rich tetradymite topological insulator $Bi_{2+x}Te_{2-x}Se$, Phys. Rev. B **86**, 165119 (2012).

[11] M. K. Fuccillo, S. Jia, M. E. Charles, and R. J. Cava, Thermoelectric properties of Bi_2Te_2Se compensated by native defects and Sn doping, J. Electron. Mater. **42**, 1246 (2013).

[12] D. Parker and D. J. Singh, Potential thermoelectric performance from optimization of hole-doped Bi_2Se_3, Phys. Rev. X **1**, 021005 (2011).

[13] W. Liu, K. C. Lukas, K. McEnaney, S. Lee, Q. Zhang, C. P. Opeil, G. Chen, and Z. Ren, Studies on the Bi_2Te_3-Bi_2Se_3-Bi_2S_3 system for mid-temperature thermoelectric energy conversion, Energy Environ. Sci. **6**, 552 (2013).

[14] D. Parker and D. J. Singh, High-temperature thermoelectric performance of heavily doped PbSe, Phys. Rev. B **82**, 035204 (2010).

[15] G. K. H. Madsen and D. J. Singh, Boltztrap. A code for calculating band-structure dependent quantities, Comput. Phys. Commun. **175**, 67 (2006).

[16] F. Tran and P. Blaha, Accurate band gaps of semiconductors and insulators with a semilocal exchange-correlation potential, Phys. Rev. Lett. **102**, 226401 (2009).

[17] D. Koller, F. Tran, and P. Blaha, Merits and limits of the modified Becke-Johnson exchange potential, Phys. Rev. B **83**, 195134 (2011).

[18] D. J. Singh, Structure and optical properties of high light output halide scintillators, Phys. Rev. B **82**, 155145 (2010).

[19] Y. S. Kim, M. Marsman, G. Kresse, F. Tran, and P. Blaha, Towards efficient band structure and effective mass calculations for III–V direct band-gap semiconductors, Phys. Rev. B **82**, 205212 (2010).

[20] D. J. Singh, Electronic structure calculations with the Tran-Blaha modified Becke-Johnson density functional, Phys. Rev. B **82**, 205102 (2010).

[21] J. A. Camargo-Martinez and R. Baquero, Performance of the modified Becke-Johnson potential for semiconductors, Phys. Rev. B **86**, 195106 (2012).

[22] D. J. Singh and L. Nordstrom, *Planewaves Pseudopotentials and the LAPW Method*, 2nd ed. (Springer, Berlin, 2006).

[23] P. Blaha, K. Schwarz, G. Madsen, D. Kvasnicka, and J. Luitz, *WIEN2k, An Augmented Plane Wave+Local Orbitals Program for Calculating Crystal Properties* (K. Schwarz, Tech. Univ. Wien, Austria, 2001).

[24] X. Chen, D. Parker, and D. J. Singh, Acoustic impedance and interface phonon scattering in Bi_2Te_3 and other semiconducting materials, Phys. Rev. B **87**, 045317 (2013).

[25] C. E. Ekuma, D. J. Singh, J. Moreno, and M. Jarrell, Optical properties of PbTe and PbSe, Phys. Rev. B **85**, 085205 (2012).

[26] D. L. Greenaway and G. Harbeke, Band structure of bismuth telluride, bismuth selenide and their respective alloys, J. Phys. Chem. Solids **26**, 1585 (1965).

[27] N. F. Hinsche, B. Y. Yavorsky, I. Mertig, and P. Zahn, Influence of strain on anisotropic thermoelectric transport in Bi_2Te_3 and Sb_2Te_3, Phys. Rev. B **84**, 165214 (2011).

[28] X. Chen, D. Parker, and D. J. Singh, Importance of non-parabolic band effects in the thermoelectric properties of semiconductors, Sci. Rep. **3**, 3168 (2013).

[29] K. Kuroki and R. Arita, Pudding mold band drives large thermopower in Na_xCoO_2, J. Phys. Soc. Jpn. **76**, 083707 (2007).

[30] D. Parker and D. J. Singh, Thermoelectric properties of $AgGaTe_2$ and related chalcopyrite structure materials, Phys. Rev. B **85**, 125209 (2012).

[31] P. Cucka and C. S. Barrett, The crystal structure of Bi and of solid solutions of Pb, Sn, Sb and Te in Bi, Acta Crystallogr. **15**, 865 (1962).

[32] R. Keller, W. B. Holzapfel, and H. Schulz, Effect of pressure on the atom positions in Se and Te, Phys. Rev. B **16**, 4404 (1977).

[33] N. Bouad, L. Chapon, R. M. Marin-Ayral, F. Bouree-Vigneron, and J. C. Tedenac, Neutron powder diffraction study of strain and crystallite size in mechanically alloyed PbTe, J. Solid State Chem. **173**, 189 (2003).

[34] C. Perez Vicente, J. L. Tirado, K. Adouby, J. C. Jumas, A. Abba Toure, and G. Kra, X-ray diffraction and ^{119} sn mssbauer spectroscopy study of a new phase in the Bi_2Se_3 − SnSe system: $SnBi_4Se_7$, Inorg. Chem. **38**, 2131 (1999).

[35] D. O. Scanlon, P. D. C. King, R. P. Singh, A. de la Torre, S. M. Walker, G. Balakrishnan, F. Baumberger, and C. R. A. Catlow, Controlling bulk conductivity in topological insulators: Key role of anti-site defects, Adv. Mater. **24**, 2154 (2012).